Solar Energy 218 (2021) 544–551

Contents lists available at ScienceDirect

Solar Energy

journal homepage: www.elsevier.com/locate/solener

Cooling of floating photovoltaics and the importance of water temperature

Torunn Kjeldstad *, Dag Lindholm, Erik Marstein, Josefine Selj

Department of Renewable Energy Systems, Institute for Energy Technology, Instituttveien 18, 2007 Kjeller, Norway

ARTICLE INFO

Keywords:
Floating PV
Cooling
Module temperature
Membrane technology
Performance
Commercial FPV system

ABSTRACT

Enhanced performance of floating PV due to water cooling is widely claimed, but poorly quantified and documented in the scientific literature. In this work, we assess the effect of water cooling for a specific technology developed by Ocean Sun AS, consisting of a floating membrane with horizontally mounted PV modules allowing for thermal contact between the modules and the water. The impact of thermal contact with water on energy yield is quantified using production data from a well-instrumented 6.48 kW installation at Skaftå, Norway. In addition, we apply a thermal model that incorporates the effect of heat transport from the module to the water to estimate the module temperature. By comparing a module string in thermal contact with water with a module string with an air gap between the water and the modules, we find that the water-cooled string had on average 5–6% higher yield compared to the air-cooled string. Also, we find that the system in thermal contact with water has a U-value of approximately 70–80 W/m^{2}K, and that it is necessary to consider the water temperature for a more accurate calculation of the module temperature.

1. Introduction

Floating photovoltaics (FPV) is growing at a rapid pace. Worldwide accumulated, installed capacity by the end of August 2020 is approximately 2.6 GW$_p$, distributed over more than 35 different countries [PV magazine]. The number of available FPV technologies and technology providers is rapidly growing. Although FPV still needs to compete with land-based PV in terms of cost [PV magazine], there are several advantages to FPV that contributes to the increased market share: FPV opens new possibilities for power production where suitable land area for PV plants is either unavailable or expensive. Power production near urban areas can also significantly reduce transmission costs. Hybridization with hydroelectric power production is also emerging as an exciting, and largely unexplored market for FPV. For hybrid applications, a range of synergies can reduce the overall power cost, such as improved PV power plant performance, shared transmission infrastructure, and improved quality of power, especially in the case of large hydropower sites that can be flexibly operated. The PV capacity can be used to boost the energy yield of the hydropower plants and may also help to manage periods of low water availability.

In the existing scientific literature, FPV is often reported to have superior performance compared to land-based PV (Golroodbari and van Sark, 2020; Kamuyu et al., 2018; Liu et al., 2018; Ranjbaran et al., 2019; Sahu et al., 2016; Suh et al., 2020). The typical explanation for the enhanced performance is that water cooling reduces the operating temperature and therefore increases the efficiency of the modules. However, the majority of these claims are either based on comparisons of ground-mounted systems and FPV systems without much monitoring (Choi, 2014; Lee et al., 2014; Suh et al., 2020; Yadav et al., 2017) or studies that have been undertaken for prototype FPV technologies in direct contact with water (Do Sacramento et al., 2015; Ho et al., 2016; Majid et al., 2014). Other studies that have found superior performance due to water cooling have utilized water as a cooling agent by either submerging the panels in water, or spraying the panels with water. Various technologies exploiting this are detailed in the reviews by Cazzaniga et al. (2018) and Dwivedi et al. (2020). The significance of FPV technology has often been under communicated when FPV cooling benefits has been summarized in reviews and reports. Although many FPV technologies may indeed have a performance superior to land-based PV due to water cooling, attempts to generalize have led to confusion with respect to the expected performance of FPV. The expectancy of extraordinary cooling for PV modules floating on structures above the water body continues to be repeated, even when several recent results and publications indicate that the cooling effect on the typical pontoon-based floaters is modest (Liu et al., 2018, 2017; Mittal et al., 2017; Oliveira-Pinto and Stokkermans, 2020). Results presented by Nobre and Peters even showed higher temperatures for the FPV modules compared to the on shore rooftop system due to reduced wind speeds on

* Corresponding author.
E-mail address: torunn.kjeldstad@ife.no (T. Kjeldstad).

https://doi.org/10.1016/j.solener.2021.03.022
Received 17 November 2020; Received in revised form 5 February 2021; Accepted 8 March 2021
Available online 21 March 2021

Fig. 1. (Ocean Sun, by permission): (a) Ocean Sun's pilot located at the west coast of Norway. Modules laying down on the membrane (b) and modules lifted by plastic pipes (c).

the water body (Nobre and Peters, 2020). A recent study by Dörenkämper et al. shows that the thermal behavior of FPV panels mounted above the water is dependent on the water footprint and closeness of the structure across different climatic conditions, which substantiates the technology dependence of the cooling effect (Dörenkämper et al., 2021).

The operating temperature of a solar cell is dependent on the irradiance and the heat exchange with its surroundings. Based on the long history of ground-mounted PV, several models have been proposed to estimate the operating cell and module temperature (Skoplaki and Palyvos, 2009). Two commonly used models are the Sandia cell and module temperature model and the Faiman module temperature model (David Faiman, 2008; King et al., 2004). As the Sandia model is purely based on empirical values found for different module structures and mounting conditions for land-based PV, it is not necessarily applicable to FPV without experimental data from the specific FPV technologies. In the model proposed by Faiman, the cell temperature, T_{cell}, is related to the ambient temperature T_{amb} and the wind speed, v_{air} through

$$T_{cell} = T_{amb} + \frac{G_{POA}}{U_0 + U_1 v_{air}}, \tag{1}$$

where U_0 is the constant heat transfer component, U_1 is the convective heat transfer component and G_{POA} the plane of array irradiance. U_0 and U_1 provide a measure of how effectively the heat absorbed by the cell is dissipated to the surroundings. In practice, the use of U_1 is often hampered by a lack of accurate wind speed measurements representative of the exact height and location of the modules, as these measurements can be difficult to obtain. Therefore, a single U-value without explicit wind dependency is often derived (implicitly assuming an average wind velocity). In Eq. (1) reflection from the module is neglected. In a more detailed expression of the module temperature the energy converted to electricity and energy reflected by the module is taken into consideration, through

$$T_{cell} = T_{amb} + \frac{G_{POA}(\tau\alpha - \eta(T))}{U_0 + U_1 v_{air}} = T_{amb} + \frac{G_{POA}(\tau\alpha - \eta(T))}{U}, \tag{2}$$

where τ is the transmittance of glazing, α is the absorbed fraction of the irradiance and $\eta(T)$ is the temperature-dependent efficiency of the solar cell. This version is applied in the widely used PV simulation tool PVsyst. In the final expression on the right-hand side, a single U-value is used without the explicit wind dependency. High U-values indicate a high level of heat exchange between the solar cell and the ambient, resulting in lower operating module temperatures. The U-value is predominantly determined by the mounting structure, although material-specific module parameters also play a role. The equation is based on steady-state heat transfer and exact calculations of the U-values are in principle possible, although this requires all relevant material parameters and the geometry of the mounting to be inserted. Alternatively, the U-values may also be derived empirically. A combination of modeling and experimental data has resulted in a set of widely used U-values for different mounting modes. PVsyst proposes a U-value of 29 W/m^{2}K for freestanding systems, a U-value of 15 W/m^{2}K for fully insulated systems, and a value of 20 W/m^{2}K for intermediate cases.

For FPV installed above the water surface without direct contact with the water, the operating temperature of the module will, as for land-based systems, predominantly be determined by the mounting structure (which greatly affects the U-value), wind and air temperature. Hence, the effects that reduce the operating temperature of such installations are lower air temperature, and changes to the flow of air underneath the modules (wind/convection). With the complexity of the calculations of U-values combined with the general lack of representative wind-data, U-values derived from experimental data is of great value. Liu et al. have recently calculated U-values without wind dependency for several FPV systems based on production data, measured ambient and module temperature (Liu et al., 2018). As expected, they found that the experimental U-values are highly dependent on the FPV technology. For robust determination of representative U-values for different technologies, experimental data from different sites and climates should be collected.

For FPV technologies which are in direct contact with water, or very close to direct contact with water, the water temperature will constitute the ambient medium on one (or both for submerged structures) sides. As water has significantly higher thermal conductivity than air ($\lambda_{water} = 0.6$ W/mK, $\lambda_{air} = 0.026$ W/mK), the water temperature and water flow will dominate for such architectures. Hence, the operating temperature of the module is therefore likely to depend on the water temperature and water flow in addition to air temperature, wind, and mounting structure. FPV technologies in direct contact with water were not included in the study undertaken by Liu et al. (2018).

In this work, we have studied the performance and cooling effect of an FPV technology patented by the company Ocean Sun AS, in which the PV modules are installed directly on a thin hydro-elastic membrane floating on the water surface (Fig. 1). Using an experimental setup with one module string resting on the canvas (water-cooled) surface and one module string lifted up from the canvas (air-cooled), we quantify the effect of water cooling. We also calculate U-values for the water-cooled string using both experimental data and a thermal model, and assess the effect of U-values and the impact of air and water temperatures when estimating operating module temperatures.

2. Experimental setup

Ocean Sun's first pilot project was installed in early 2017 and is located at Skaftå on the Norwegian west coast (60.45, 5.62). Although Ocean Sun more recently has installed several significantly larger systems globally, the first pilot is not in commercial operation and is hence an ideal site to perform experimental studies. It consists of two strings of twelve Trina Solar 270 W Duomax (glass/glass) modules each connected to a Fronius Primo 6.0–1 inverter. The modules have a PMAX temperature coefficient of 0.41%/°C, as specified in the datasheet. A picture of the pilot is provided in Fig. 1 (a). The pilot was established in April 2017, but the current modules from Trina Solar were installed in May 2018.

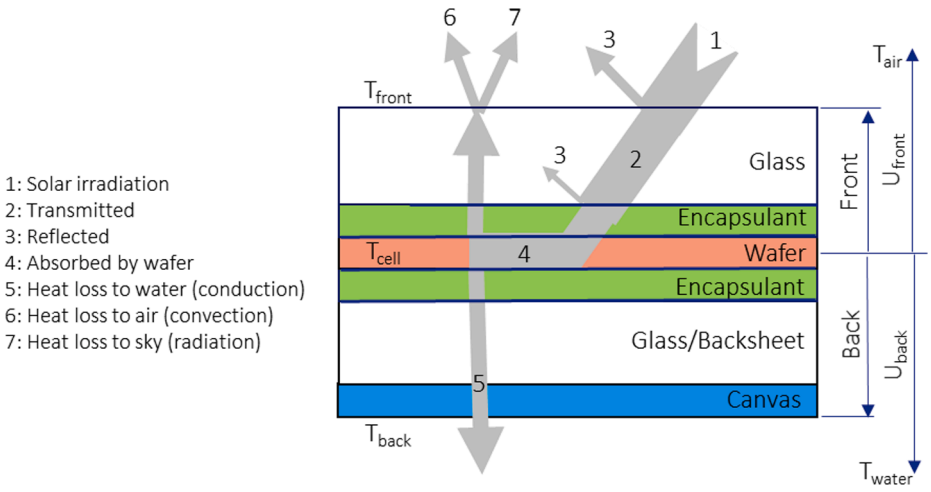

Fig 2. Heat flows and heat exchange modes in the thermal model.

Table 1
Coefficients applied in the thermal model.

Heat transfer coefficients (air, sky and water):	
$h_{air} = 2.8 + 3 \cdot v_{air}$ (Watmuff et al., 1977)	$T_{sky} = 0.0552 T_{air}^{1.5}$ (Swinbank, 1963)
$h_{sky} = \varepsilon\sigma(T_{front} + T_{sky})\left(T_{front}^2 + T_{sky}^2\right)$	$Re = v_{water} L/\nu$
$h_{water} = Nu \cdot \lambda_{water}/L$	$Nu = 0.664 Re^{1/2} Pr^{1/3}$ (laminar) (Incropera et al., 1990)

h_i = Heat transfer coefficient (convection to air or water, thermal radiation to sky).
T_i = Temperature (module front, air or sky).
v_i = Velocity (air or water).
ε = Emissivity of the front glass.
$\sigma = 5.67 \cdot 10^{-8}$ W/m^{2}K^4 (Stefan-Boltzmann's constant).
ν = Kinematic viscosity of water.
L = Length scale (size of module).
λ_{water} = Thermal conductivity of water.
Re = Reynolds number (water).
Pr = Prandtl number (water).

The modules at Skaftå have the junction box on the rear side. This is changed for the new Ocean Sun installations, where the modules have the junction box on the side to improve the cooling further. Although the modules are separated from the water by the membrane, rain water must be removed to avoid submerging the panels in water. This is done through a pumping system that quickly removes any surface water. In February 2019, one string was elevated from the canvas by the insertion of three 32 mm diameter plastic pipes underneath each of the modules (air-cooled) as shown in Fig. 1 (c). The other string was left in contact with the membrane (water-cooled) as shown in Fig. 1 (b).

Additionally, the pilot was instrumented to enable precise monitoring and analysis of the performance. The analysis is based on data for power, ambient temperature, water temperature, module temperature, and wind speed. Power data was logged by the Fronius inverter. Irradiation measurements were performed using a crystalline silicon reference cell. Wind velocity was measured with a Fronius Cup anemometer with a resolution of 1 m/s and a threshold of 2.5 m/s. Ambient and water temperature was measured with Fronius PT1000 sensors with tolerances of ±0.8 °C. Module temperatures were measured by a total of four RS PRO PT100 temperature sensors with tolerances of ±0.3 °C. These were attached to the rear side of two modules in the water-cooled string and two modules in the air-cooled string. One of the temperature sensors detached during the measurement campaign and only the remaining three temperature measurements were used in the analysis. Complete module temperature data are available for May and June. All values are averages over five-minute intervals. Due to the local topography, some shading is present in the morning and afternoon. To avoid production differences due to shading, only times between 9 and 15 are included in the data analysis.

3. Thermal model

The expressions for module temperature shown in Eqs. (1) and (2) are derived for a land-based system, where air constitutes the surrounding medium, and for FPV this is not necessarily the case. Based on a steady-state heat balance, a thermal model for computing module temperatures and heat loss coefficients of FPV systems has been developed (Lindholm et al., 2020). For a module fixed to a large canvas floating on a water body, a steady-state heat balance can be written as

$$(\tau\alpha - \eta) \cdot G_{POA} = G_a + G_w. \quad (3)$$

In Eq. (3) the terms on the left-hand side represent irradiated heat absorbed by the cell, G_a is the heat flow from the cell to the air-cooled module front surface, G_w is the corresponding heat flow from the wafer to the water-cooled module back surface. For simplicity, we neglect heat absorbed by the upper glass and assume that all absorbed heat is absorbed by the wafer. Fig. 2 shows the heat flows and heat exchange modes that are considered by the model. At the front surface, heat is exchanged both by convection and thermal radiation. Heat conducted downwards through the canvas is transferred to the water by convection.

As indicated in Fig. 2, the thermal model divides the modules into

Table 2
Heat transfer coefficients and sky temperature.

Module upper half:	Module lower half:
$\frac{1}{A_{front}} = \left(\frac{\Delta s_c}{2\lambda_c}\right) + \sum_i \left(\frac{\Delta s_{i,front}}{\lambda_{i,front}}\right)$	$\frac{1}{A_{back}} = \left(\frac{\Delta s_c}{2\lambda_c}\right) + \sum_i \left(\frac{\Delta s_{i,back}}{\lambda_{i,back}}\right)$
$B_{front} = A_{front} + h_{air} + h_{sky}$	$B_{back} = A_{back} + h_{water}$
$C_{front} = h_{air}T_{air} + h_{sky}T_{sky}$	$C_{back} = h_{water}T_{water}$

Δs_i = Thickness of module layer *i* (cell, encapsulant, glass or canvas).
λ_i = Thermal conductivity of module layer *i*.
h_i = Heat transfer coefficient (convection to air or water, thermal radiation to sky).
T_i = Temperature (air, water or sky).

two parts, one upper part and another lower part. Details of derivation made for the thermal model is given in Ref. 16 and only the main equations are presented here. The temperature of the solar cell inside the module (T_{cell}), as well as the temperatures at the front (T_{front}) and back (T_{back}) of the module, as shown in Fig. 2, are computed from the three equations:

$$T_{cell} = \frac{B_{front}B_{back}(\tau\alpha - \eta)G_{POA} + A_{front}B_{back}C_{front} + A_{back}B_{front}C_{back}}{B_{front}B_{back}(A_{back} + A_{front}) - A_{back}^2 B_{front} - A_{front}^2 B_{back}}. \quad (4)$$

$$T_{back} = \frac{A_{back}T_{cell} + C_{back}}{B_{back}}. \quad (5)$$

These equations include the coefficients A_i, B_i, and C_i that depend on the bill of materials (BOM) and on the heat transfer coefficients. The coefficients are defined in Table 1. The index *front* refers to the module upper half, while *back* refers to the lower half. The various layers in the module that are accounted for in the model are shown in Fig. 2. The applied heat transfer coefficients and the model applied to compute the sky temperature are presented in Table 2.

The thermal model computes the overall U-value of the component representing the heat loss through the module upper half and that for the lower half. The proposed equation is

$$U(T_{cell} - T_{fluid}) = U_{front}(T_{cell} - T_{air}) + U_{back}(T_{cell} - T_{water}), \quad (6)$$

where U is the overall U-value and T_{fluid} is the associated fluid temperature. The U-value components are computed from

$$U_{front} = \frac{A_{front}(h_{air} + h_{sky})}{A_{front} + h_{air} + h_{sky}}. \quad (7)$$

$$U_{back} = \frac{A_{back}h_{water}}{A_{back} + h_{water}}. \quad (8)$$

The overall U-value is computed as the sum of the two components, i.e.

$$U = U_{front} + U_{back}. \quad (9)$$

The fluid temperature associated with the overall U-value is an artificial fluid temperature based on weighting with respect to the U-value components. It is closer to the fluid temperature on the dominant heat flow side than to the other. This temperature is computed from Eq.

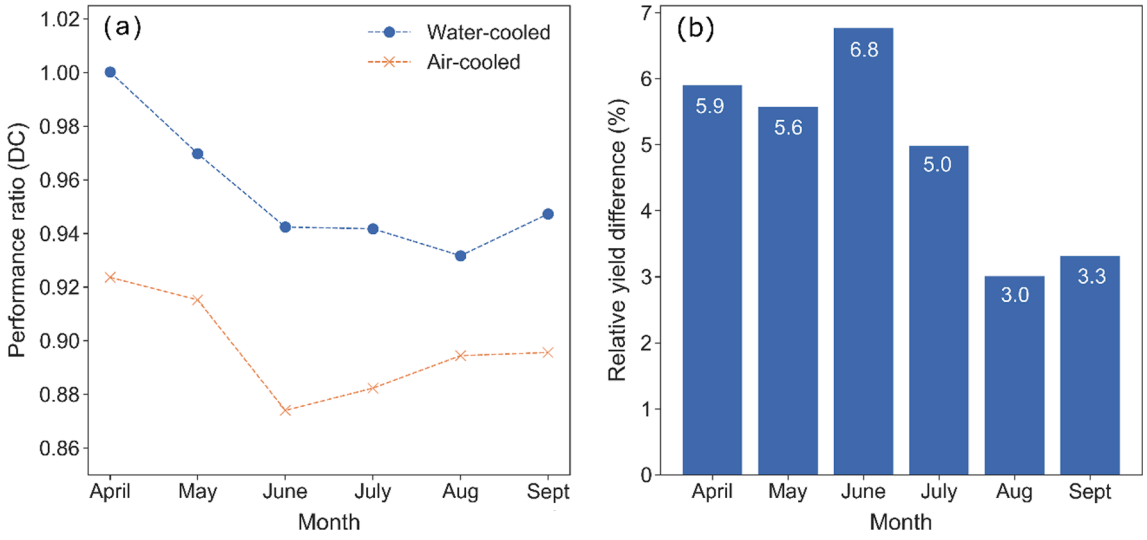

Fig. 3. (a) Performance ratio of the two strings from April to September, (b) irradiance weighted relative yield difference between the two strings.

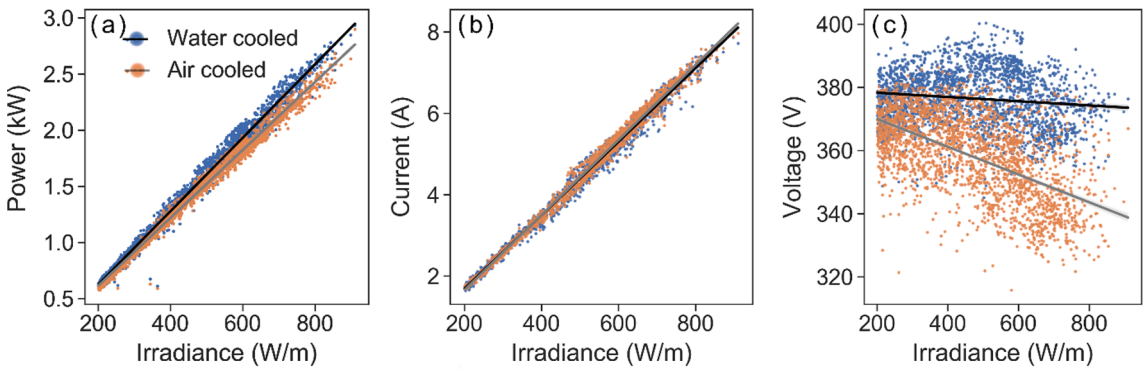

Fig. 4. Power (a), current (b) and voltage (c) aggregated to a 15 min median as a function of irradiance for the water and air cooled strings.

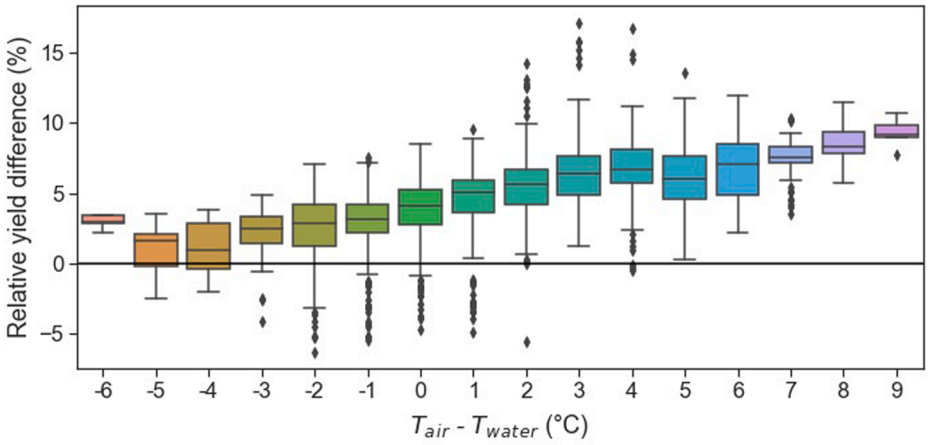

Fig. 5. Relative yield difference as a function of difference in air and water temperature for 15 min aggregated median. The box extends from the lower to upper quartile values of the data, with a line at the median. The whiskers extend from the box to show the range of the data. Flier points are those past the end of the whiskers. Note that the temperature differences of −5 °C and −6°C only contains 5 data points each.

(6) as

$$T_{fluid} = \frac{U_{front}}{U_{front} + U_{back}} T_{air} + \frac{U_{back}}{U_{front} + U_{back}} T_{water}. \quad (10)$$

4. Results

4.1. Measured performance

The string performance ratio (*PR*) is calculated by $PR = \Sigma E_{DC} / \Sigma(P_{STC}(G_{POA}/G_{STC}))$, where E_{DC} is the produced energy, P_{STC} is the rated power, and G_{STC} is the irradiance at standard conditions (1000 W/m^2) and the overall PR per month for the two strings is given in Fig. 3 a). This clearly shows improved performance for the string that is resting on the canvas. The PR values are relatively high for both strings. This is to some degree related to the cold climate of the site, a commonly observed situation for PV systems in Norway. A decrease in PR in the summer is due to an increase in both air and water temperature. To compare the performance of the two strings, the irradiance weighted relative yield difference is calculated by $\Sigma(((E_{DC,water}\text{-}E_{DC,air})/E_{DC,air})*G_{POA})/\Sigma\ G_{POA})$, where $E_{DC,water}$ and $E_{DC,air}$ is the energy produced by the water-cooled and air-cooled string respectably. Fig. 3 b) shows the irradiance weighted relative yield difference between the strings for April – September 2019. For all months, the string that is in direct contact with the canvas has significantly higher production compared to the elevated string. Note that this difference is achieved with an air gap of only 32 mm between the canvas and the modules for the air-cooled string. An increase in air and water temperature could result in a decreased yield difference, as is seen for August and September. However, both water and air temperatures in August and September were similar to those in May and June. Therefore, the decreased difference in relative yield in August and September is likely due to mispositioning of the plastic pipes used to elevate the air-cooled string. Because the plastic pipes were not adjusted during the experiment, they may have moved somewhat due to wind and waves experienced in this period. Displacement of the pipes would lead to a smaller air gap between the module and canvas, possibly resulting in partial thermal contact with water.

Fig. 4 shows the power, current, and voltage aggregated to a 15 min median plotted as a function of POA irradiance. While the current is similar for the two strings, there is a clear difference in the voltage characteristics with increasing irradiance, shown in Fig. 4 c). For the water-cooled string, the voltage is less affected by an increase in irradiance compared to the air-cooled string. A voltage drop with increasing irradiance is commonly seen for land-based PV and is a result of an increase in operating temperature. Hence, the difference in power between the two strings comes from a difference in operating voltage due to different operating temperatures for the two modules.

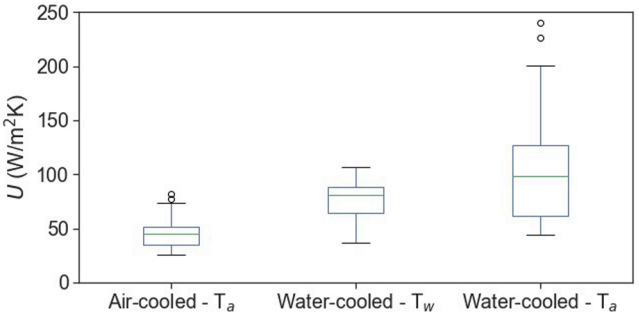

Fig. 6. U-values calculated from production data for the air-cooled string using the air temperature as T_{amb}, and the water-cooled string where both water and air temperature has been used as $T_{amb,}$ noted T_w and T_a respectively. The box extends from the lower to upper quartile values of the data, with a line at the median. The whiskers extend from the box to show the range of the data. Flier points are those past the end of the whiskers.

As shown in Fig. 4 (a), the difference in power increases with increasing irradiance. The difference in yield also increases with increasing temperature difference between water and air, as shown in Fig. 5. Here the relative yield difference is plotted as a function of $T_{air} - T_{water}$, and negative values imply that the air is colder than the water. Due to increased thermal transport between the modules and water, the relative yield difference is positive even at times where the air is colder than the water. From Fig. 5, we can conclude that a larger temperature difference results in a larger relative yield difference, indicating that both air and water temperatures impact the energy yield for technologies in thermal contact with water.

4.2. U-value estimates

Production data can be used to calculate the system U-value if the system is sufficiently instrumented to measure irradiance, air and module temperature, and wind speed. For this study, the effect of wind speed is not investigated because the system experienced very little wind (between 0 and 1 m/s) in the periods from which the U-value is computed. The existing U-value estimates provided in simulation tools such as PVsyst and in previous FPV literature are calculated using the air temperature as T_a. As shown in Fig. 4, the water temperature has a large impact on the system yield, through its effect on the operating module

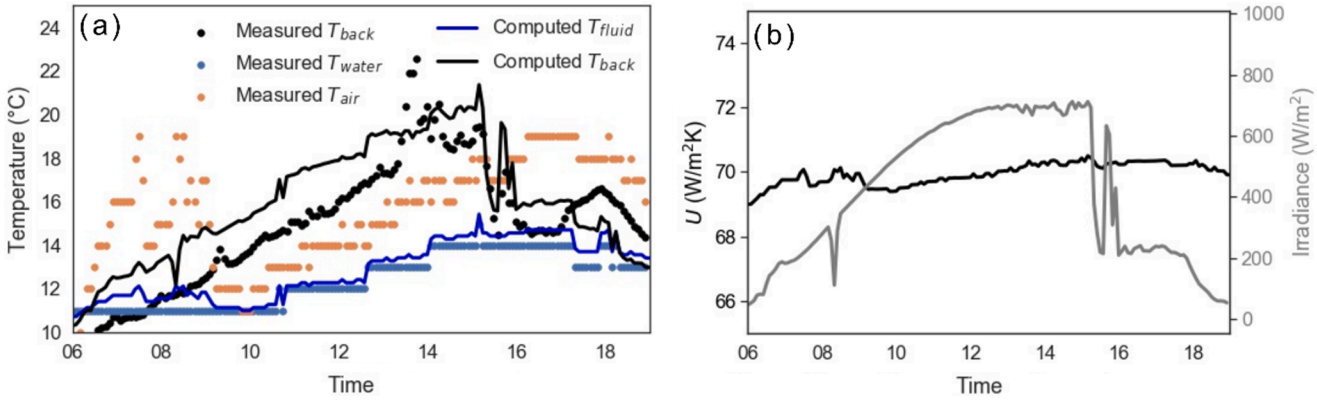

Fig. 7. Computed versus measured values at Skaftå 15th May 2019. (a) Measured and computed temperatures, (b) overall U-value (computed) and irradiation (measured).

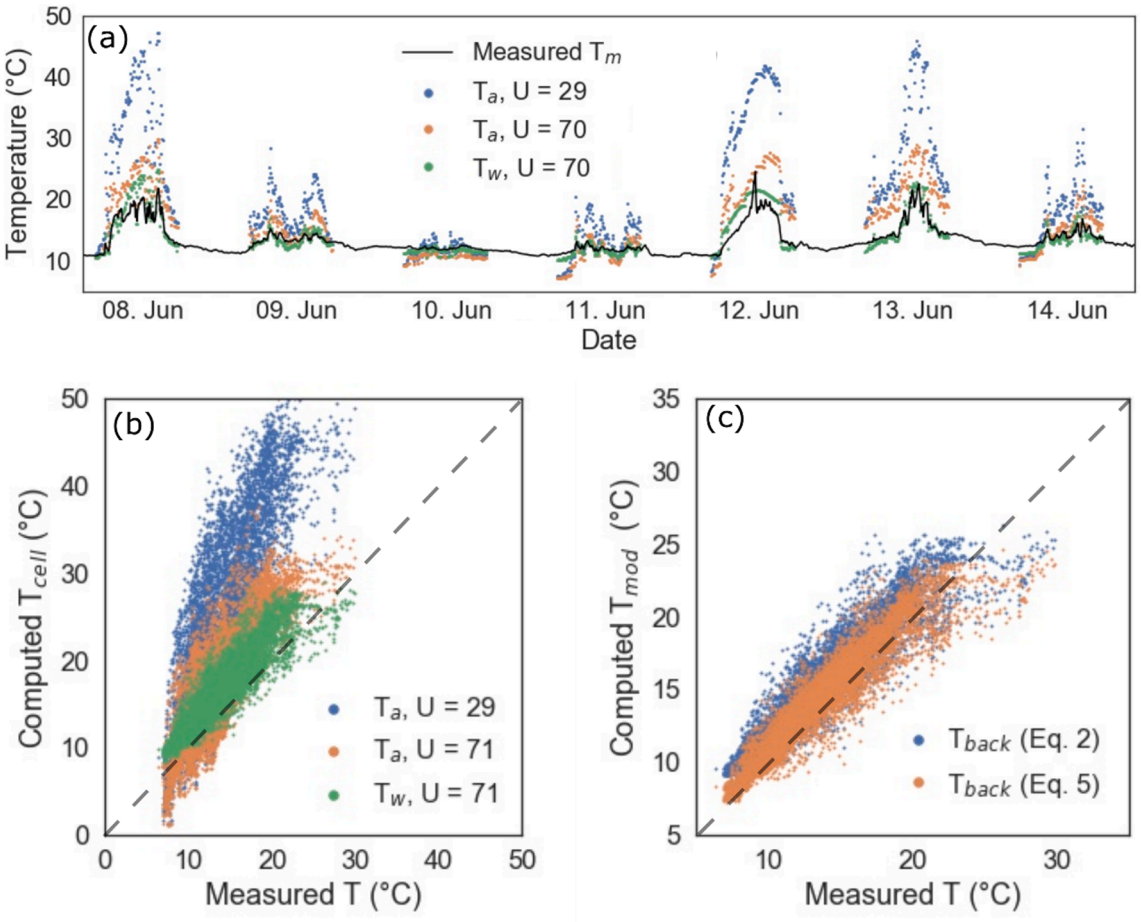

Fig. 8. (a) Measured and computed module and cell temperatures in the beginning of June. The cell temperatures have been computed using Eq. (2) with T_{air} and T_{water} as T_{amb} and using different U-values. In (b) the computed T_{cell} for the whole period (May and June) are plotted against measured T_{back} using Eq. (2) with T_{air} and T_{water} as T_{amb} and different U-values. (c) compares computed T_{back} obtained from Eq. (5) and computed T_{back} obtained from Eq. (2) ($T_{amb} = T_{water}$ and U = 71 W/m^{2}K) where cell and module temperature difference has been taken into consideration(King et al., 2004).

and cell temperatures. Results from the thermal model show that heat exchange is predominantly between water and module. Ideally, a full thermal model taking both air and water temperature should be developed and used for precise energy yield calculations. Until such models are available and integrated into software such as PVsyst, a practical approximation is utilizing Eq. (2) for U-value calculations and use the water temperature as T_a. Fig. 6 shows U-values obtained from production data and measured temperatures for both the water-cooled and the air-cooled string. In our calculations, the efficiency (η) is estimated based on production data and measured irradiance. As the expression for the U-value is given for steady-state conditions, only clear sky periods have been used for the calculations. U-values for the air-cooled string have been calculated by using the air temperature as T_{amb}, and the median value $U = 46$ W/m^{2}K, represented by the line in the box plot. For the water-cooled string, an estimate of the U-value is obtained by using the water temperature as T_{amb}. This results in a U-value of 81 W/m^{2}K.

For illustration, we also include the U-value of the water-cooled string when the air temperature is used as ambient. When the air temperature is used to calculate the U-values for the water-cooled string it will provide misleading results as it attempts to strongly correlate variables that are weakly correlated. This results in a large spread in U-values between – 3000 W/m^{2}K and 2000 W/m^{2}K. Therefore, axis limitations have been used and some of the outliers present for the U-value for the water-cooled string using air temperature as T_{amb} are not included in the figure. Negative U-values, which are computed even at high irradiance levels, are a result of events where the operating temperature is lower than the air temperature, occurring due to the active cooling of water. For a land-based system, this would not occur during high levels of irradiance.

With the assumption of a constant wind velocity of 1 m/s and a corresponding calm water velocity of 0.1 m/s, the thermal model introduced in Section 3 can be used to compute the overall U-value and the module temperatures. For an arbitrary hot summer day in Norway with high irradiance, results are shown in Fig. 7. The figure on the left-hand side shows that the computed and measured module back surface temperatures correspond well. It also shows that the weighted fluid temperature computed from Eq. (10) is significantly closer to the measured water temperature than the measured air temperature. Together with the measured irradiation, Fig. 7 b) shows the overall U-value computed from Eq. (9). Despite the fact the irradiation varies a lot throughout the day, the U-value remains relatively constant. Increased irradiation accompanied by increased air and water temperature has a modest influence on the heat transfer coefficients through the temperature-dependent fluid properties. The average U-value through the day was computed to be 71 W/m^{2}K, which agrees well with the value derived in the analysis based on the production data.

4.3. Thermal modelling of system temperatures

To evaluate the applicability of the U-values computed from the thermal model over a longer time period, cell temperatures have been computed using measured weather data time series from the period April to June as input and compared to measured module temperature time series. Fig. 8 a) and b) shows that by using Eq. (2) and a U-value of 29 W/m^{2}K, as is typically done in simulation software such as PVsyst, the module temperature is significantly overestimated. In this case, the expected yield would be underestimated as higher operating temperatures reduce the power output. If Eq. (2) is to be used to calculate the cell temperature, the best estimate of the cell temperature is obtained by using the water temperature as T_{amb}. It should be noted that the cell temperature computed from Eq. (2) is consistently higher than the measured module temperature, which is expected as the temperature is measured at the rear side of the module. In Fig. 8 c) the computed temperature for T_{back}, using Eq. (5) is shown together with the cell temperature computed from Eq. (2) ($U = 71$ W/m^{2}K and $T_{amb} = T_{water}$). To account for the difference between cell and backside temperature, the Sandia cell temperature model has been applied: $T_{cell} = T_{back} - (G_{POA}/G_{STC})x\Delta T$, and $\Delta T = 3^\circ$ (King et al., 2004). This shows that the module temperature is even more accurately described by using the thermal model which considers both air and water temperatures, compared to the more simplified expression where only water temperature is considered.

5. Conclusion

We have analyzed the performance and quantified the cooling effect of a patented FPV technology developed by Ocean Sun AS. The performance of two module strings on a pilot installation at Skaftå were directly compared and showed that a string directly in contact with the membrane resting on the water body on average exhibits a 5–7% higher yield than the string that was cooled by air in the months May to July. The yield difference is dependent on the difference in air and water temperature. The water-cooled string outperforms the air-cooled string even when the water temperature is warmer than air due to more efficient heat transport. Our study validates claims that some FPV technologies provide performance enhancements due to cooling. We have estimated the U-values for the system using thermal models based on (1) production data and (2) measured module temperatures. Both methods provide a U-value of approximately 70–80 W/m^{2}K for the Ocean Sun technology, where the PV modules are mounted directly on a floating membrane, allowing for thermal contact between module and water. Computations of the module temperature from air and water temperature show that for this technology, it is insufficient to increase the U-value when estimating module temperatures, and it is necessary to include the water temperature in the calculations.

Declaration of Competing Interest

The authors declare that they have no known competing financial interests or personal relationships that could have appeared to influence the work reported in this paper.

Acknowledgements

This work was supported by the Norwegian Research Council through project 309820. We like to thank Børge Bjørneklett and Sigmund Bragstad from Ocean Sun AS for facilitating the project and sharing the production data. In addition, we would like to thank Ida Haugem Lereng and Philip De Paoli who helped set up the experiment.

References

Cazzaniga, Cicu, Rosa-Clot, Rosa-Clot, Tina, Ventura, 2018. Floating photovoltaic plants: performance analysis and design solutions. Renew. Sustain. Energy Rev. 81, 1730–1741. https://doi.org/10.1016/j.rser.2017.05.269.

Choi, Y.K., 2014. A study on power generation analysis of floating PV system considering environmental impact. Int. J. Softw. Eng. its Appl. 8, 75–84. https://doi.org/10.14257/ijseia.2014.8.1.07.

Dwivedi, Pushpendu, Sudhakar, Soni, Archanace, Solomin, Kirpichnikova, 2020. Advanced cooling techniques of P.V. modules: a state of art. Case Stud. Therm. Eng. 21, 100674. https://doi.org/10.1016/j.csite.2020.100674.

Faiman, David, 2008. Assessing the outdoor operating temperature of photovoltaic modules. Prog. Photovoltaics Res. Appl. 16, 307–315.

Do Sacramento, E.M., Carvalho, P.C.M., De Araújo, J.C., Riffel, D.B., Da Cruz Corrêa, R. M., Neto, J.S.P., 2015. Scenarios for use of floating photovoltaic plants in Brazilian reservoirs. IET Renew. Power Gener. 9, 1019–1024. https://doi.org/10.1049/iet-rpg.2015.0120.

Dörenkämper, M., Wahed, A., Kumar, A., de Jong, M., Kroon, J., Reindl, T., 2021. The cooling effect of floating PV in two different climate zones: a comparison of field test data from the Netherlands and Singapore. Sol. Energy 214, 239–247. https://doi.org/10.1016/j.solener.2020.11.029.

Golroodbari, S.Z., van Sark, W., 2020. Simulation of performance differences between offshore and land-based photovoltaic systems. Prog. Photovoltaics Res. Appl. 28, 873–886. https://doi.org/10.1002/pip.3276.

Ho, C.J., Chou, W.L., Lai, C.M., 2016. Thermal and electrical performances of a water-surface floating PV integrated with double water-saturated MEPCM layers. Appl. Therm. Eng. 94, 122–132. https://doi.org/10.1016/j.applthermaleng.2015.10.097.

Incropera, F.P., Bergman, T.L., DeWitt, D.P., Lavine, A.S., 1990. Introduction to Heat Transfer. John Wiley & Sons, Hoboken, NJ.

Kamuyu, W.C.L., Lim, J.R., Won, C.S., Ahn, H.K., 2018. Prediction model of photovoltaic module temperature for power performance of floating PVs. Energies 11. https://doi.org/10.3390/en11020447.

King, D.L., Boyson, W.E., Kratochvil, J.A., 2004. Photovoltaic array performance model, SANDIA Report SAND2004-3535. Sandia Rep. No. 2004-3535 8, 1–19.

Lee, Y.G., Joo, H.J., Yoon, S.J., 2014. Design and installation of floating type photovoltaic energy generation system using FRP members. Sol. Energy 108, 13–27. https://doi.org/10.1016/j.solener.2014.06.033.

Lindholm, D., Kjeldstad, T., Selj, J., Marstein, E., Fjær, H.G., 2020. The heat loss coefficient computed for floating PV modules. Manuscr. Submitt. Publ.

Liu, H., Krishna, V., Lun Leung, J., Reindl, T., Zhao, L., 2018. Field experience and performance analysis of floating PV technologies in the tropics. Prog. Photovoltaics Res. Appl. 26, 957–967. https://doi.org/10.1002/pip.3039.

Liu, L., Wang, Q., Lin, H., Li, H., Sun, Q., Wennersten, R., 2017. Power generation efficiency and prospects of floating photovoltaic systems. Energy Procedia 105, 1136–1142. https://doi.org/10.1016/j.egypro.2017.03.483.

Majid, Z.A.A., Ruslan, M.H., Sopian, K., Othman, M.Y., Azmi, M.S.M., 2014. Study on performance of 80 watt floating photovoltaic panel. J. Mech. Eng. Sci. 7, 1150–1156. https://doi.org/10.15282/jmes.7.2014.14.0112.

Mittal, D., Saxena, B.K., Rao, K.V.S., 2017. Comparison of floating photovoltaic plant with solar photovoltaic plant for energy generation at Jodhpur in India. In: IEEE Int. Conf. Technol. Adv. Power Energy (TAP Energy) 1–6. 10.1109/TAPENERGY.2017.8397348.

Nobre, A.M., Peters, I.M., 2020. No Title. In: On Module Temperature in Floating PV Systems. p. Presented at conference.

Oliveira-Pinto, S., Stokkermans, J., 2020. Assessment of the potential of different floating solar technologies – Overview and analysis of different case studies. Energy Convers. Manag. 211, 112747 https://doi.org/10.1016/j.enconman.2020.112747.

Ranjbaran, P., Yousefi, H., Gharehpetian, G.B., Astaraei, F.R., 2019. A review on floating photovoltaic (FPV) power generation units. Renew. Sustain. Energy Rev. 110, 332–347. https://doi.org/10.1016/j.rser.2019.05.015.

Sahu, A., Yadav, N., Sudhakar, K., 2016. Floating photovoltaic power plant: a review. Renew. Sustain. Energy Rev. 66, 815–824. https://doi.org/10.1016/j.rser.2016.08.051.

Skoplaki, E., Palyvos, J.A., 2009. Operating temperature of photovoltaic modules: a survey of pertinent correlations. Renew. Energy 34, 23–29. https://doi.org/10.1016/j.renene.2008.04.009.

Suh, J., Jang, Y., Choi, Y., 2020. Comparison of electric power output observed and estimated from floating photovoltaic systems: a case study on the hapcheon dam. Korea. Sustain. 12 https://doi.org/10.3390/su12010276.

Swinbank, W., 1963. Long-wave radiation from clear skies. Q. J. R. Meteorol. Soc. 89, 339–348.

Watmuff, J.H., Charters, W.W.S., Proctor, D., 1977. Solar and wind induced external coefficients solar collectors. Rev. Int. Heliotech. 2, 56.

Yadav, N., Gupta, M., Sudhakar, K., 2017. Energy assessment of floating photovoltaic system. In: Int. Conf. Electr. Power Energy Syst. ICEPES 2016, pp. 264–269. 10.1109/ICEPES.2016.7915941.